

# Analysis and Testing of Lithium-Ion Battery Materials

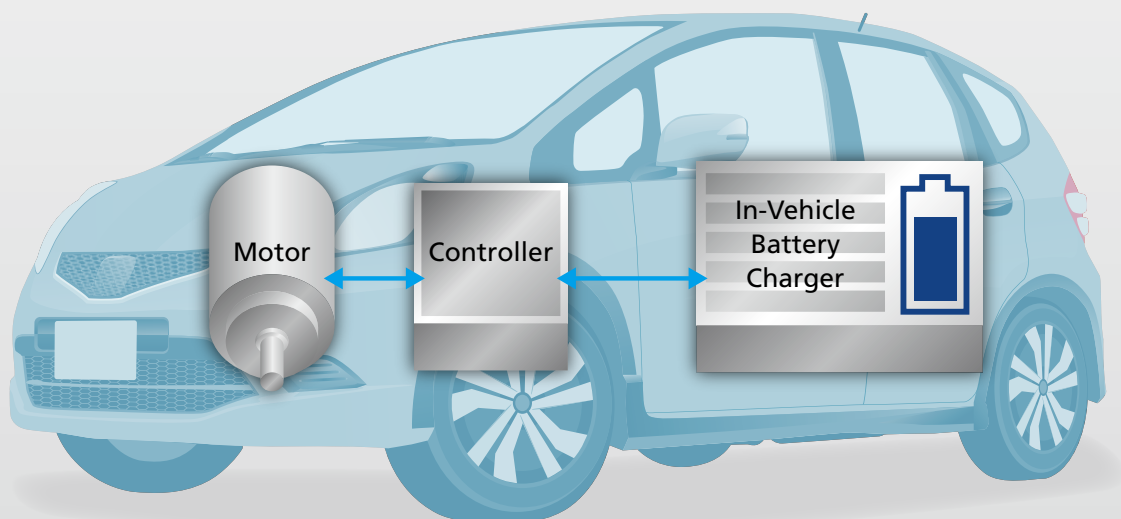


# Multifaceted Solutions for Improving Performance and Quality of Lithium-Ion Secondary Batteries

In the field of transport equipment, which accounts for approximately 20% of CO<sub>2</sub> emissions, there is a strong demand for expanding the use of electric vehicles with little environmental load, such as electric vehicles (EV) and hybrid vehicles (HEV and PHEV).

Achieving this goal will require both a reduction in the cost of lithium-ion secondary batteries, which account for a large portion of car body prices, an improvements in performance, such as extending the travel distance and shortening the charging time. In addition, issues related to high-energy density,

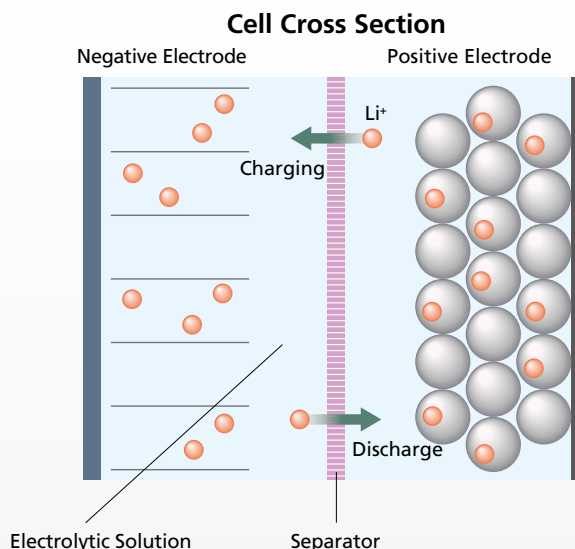
long life, and safety must be resolved. Research institutes around the world are making all-out efforts in research and development and demonstration projects to address these issues. Shimadzu provides a diverse array of analytical and measuring equipment for research and development to material property evaluation, product quality control, and degradation analysis. These technologies will allow researchers and manufacturers around the world to address issues related to lithium-ion secondary batteries and improve performance and quality.



## Principle of Lithium-Ion Secondary Batteries

A lithium-ion battery consists of a positive electrode, a negative electrode, an electrolytic solution, and a separator. When a battery is charged, lithium ions escape from the positive electrode made of metal oxide, pass through the electrolytic solution, reach the negative electrode, and accumulate.

During discharge, lithium ions emitted from the negative electrode move to the positive electrode through the electrolytic solution. This enables an electric current to flow to the outside.



## Applications for Analysis and Testing of Lithium-Ion Battery Materials

### Positive Electrodes - Negative Electrodes

State Change in Charge and Discharge Process of Ternary Positive Electrode Materials of Ni, Co and Mn : Chemical Bond Analysis System	P.4
Changes in Chemical Bonding States of Li-Rich Cathode Materials : Chemical Bond Analysis System	P.4
Shape Observation of Binder for Negative Electrodes in Electrolytic Solution/Force Curve Measurement : Scanning Probe Microscope	P.8

### Separators

Thermal Characterization : Differential Scanning Calorimeter, Thermomechanical Analyzer	P.9
Puncture Strength Test : Universal Testing Machine	P.9

### Electrolytic Solution

Analysis of Electrolytic Solution and Gases Generated from Cells : Gas Chromatograph Mass Spectrometer	P.6
Analysis of Degradation Products in Electrolytes (Deteriorated Electrolytes) : Suppressor Ion Chromatograph for Anion Analysis	P.7

### Cells - Modules

Observation of 18650 Lithium-Ion Secondary Batteries : X-ray CT System	P.5
Observation of In-Vehicle Lithium-Ion Secondary Batteries : X-ray CT System	P.5
Observation of Lithium Polymer Batteries : X-ray CT System	P.5

### All-Solid-State Batteries

Depth Profiling of LiPON Films (Solid Electrolytes) : X-ray Photoelectron Spectroscopy	P.10
Particle Size Distribution of Raw Material Powder (Solid Electrolytes) : Dynamic Particle Image Analysis System (DIA)	P.11
Compressive Strength of Raw Material Powder (Solid Electrolytes) : Micro Compression Tester (MCT)	P.11

# Analysis of Positive Electrodes

## State Change in Charge and Discharge Process of Ternary Positive Electrode Materials

Xspecia™

Lithium-ion secondary batteries are used not only in portable electronic devices but also in a wide range of products, such as electric vehicles, aircraft, and power supplies for power storage. In line with this, high output capacity, long life, and improved safety are required. In order to improve performance, it is important to accurately evaluate the chemical bonding states (valence change) of positive electrodes accompanying lithium-ion migration.

Here, measurement examples of changes in the chemical bond states in the charge and discharge processes of ternary and Li-rich cathode materials using the Xspecia chemical bond analysis system are introduced.



### Chemical Bond Analysis System for Positive Electrode Materials in Lithium-Ion Batteries Xspecia™

With excellent resolution, chemical shifts due to changes in chemical states can be observed. These energy changes are converted into state changes called "valence number". Because of this, the state changes of real samples can be quantitatively and directly analyzed. The chemical states of the positive electrode materials can be quickly and easily evaluated in a laboratory without the assistance of large external facilities.

Fig. 1 shows state changes in the ternary positive electrode materials (Ni, Co, Mn) obtained from Xspecia in an initial state (before charging), at a 50% charge, at full charge, at a 50% discharge, and at full discharge.

The change in the chemical bonding state around Ni was largest in the charge and discharge processes and changed from 3 in the initial state to 3.6 in the full charge. In addition, a ternary and quaternary mixture occurred at the time of charging. The chemical bonding state around Co also varied slightly from 3 to 3.2. Mn hardly changed.

The results of X-ray Absorption Fine Structure measurements on similar samples at SPring-8 BL14B2 are shown in Fig. 2. Measurements were evaluated at the position of the spectrum as it rose in comparison with divalent and trivalent standard samples.

Before charging (SOC-0: Green Line), the rising point was close to that of the trivalent standard sample (LiNiO<sub>2</sub> (III): Black Solid Line), and in full charge (SOC-100: red line), the rising point was higher (move to the right side) than that of the trivalent standard sample, and the valence increased. This indicates there was a good correlation with the increase in the valence after charging (SOC-100) measured by Xspecia in Fig. 1

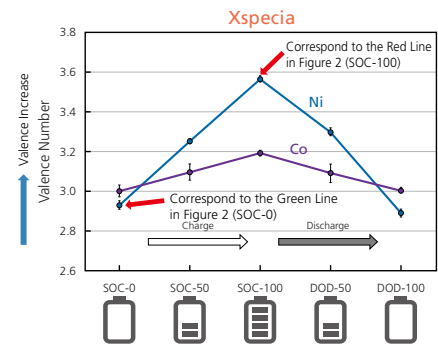


Fig. 1 Change in Chemical Bonding State of Ternary Positive Electrode Materials

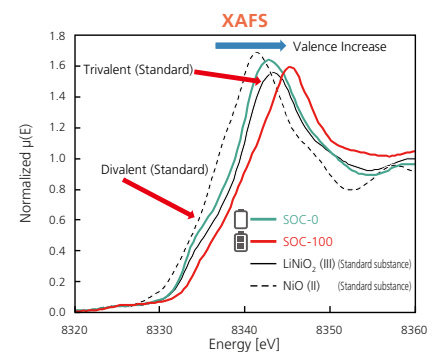


Fig. 2 XAFS Measurement Results of Ternary Positive Electrode Materials

## Change in Chemical Bonding State of Li-Rich Cathode Materials Xspecia

Understanding chemical state changes is necessary to increase the capacity of lithium-ion batteries. Fig. 3 shows the results of a change in the chemical bonding state of Li<sub>x</sub>Ni<sub>0.2</sub>Mn<sub>0.6</sub>O<sub>2</sub>, in which a part of the transition metal layer in the layered rock salt-type structure was replaced with Li, during the charge and discharge processes using Xspecia.

Changes in the chemical bonding state of Mn and Ni were evaluated in 4 states, i.e., initial state, 50% state of charge, 100% state of charge, and 100% state of discharge (reinitialization state). Chemical state changes corresponding to charge and discharge were observed.

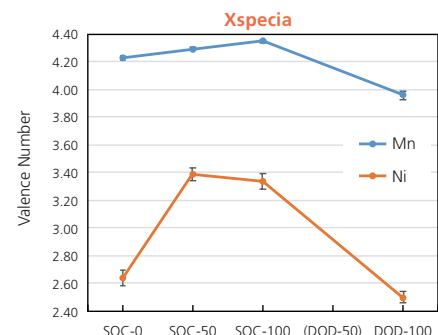


Fig. 3 Change in Chemical Bonding State of Li-Rich Cathode Materials

# Non-Destructive Observation Inside Batteries

## Observation of 18650 Lithium-Ion Secondary Batteries inspeXio SMX-225CT FPD HR Plus



Micro Focus X-Ray CT System  
inspeXio SMX-225CT FPD HR Plus

The basic dimensions of a 18650 inch lithium-ion battery are a cylindrical shape with a diameter of 18 mm and a length of 65 mm. The manufacturing cost is reduced by unifying the shape. Currently, methods for enlarging containers are being developed in order to increase the number of windings inside the containers and to increase the capacity required for automotive applications. In Fig. 1, fine deformation of the electrodes is clearly observed while observing the entire battery. In addition, in Fig. 2, the resin separators between the positive and negative electrodes, which are difficult to observe, can be clearly confirmed.

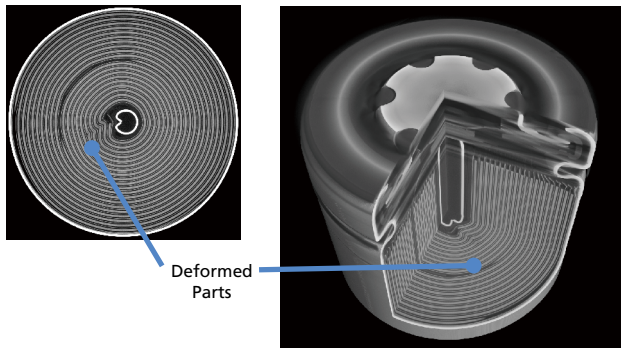


Fig. 1 18650 Lithium-Ion Battery

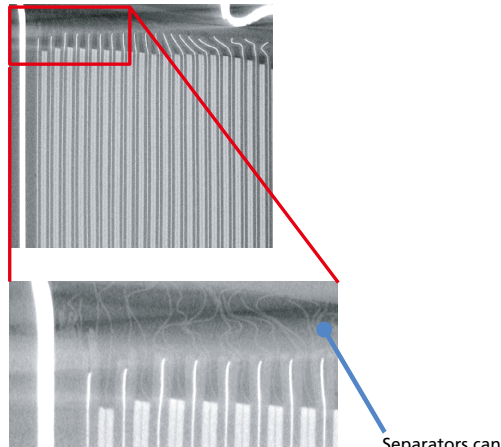


Fig. 2 18650 Lithium-Ion Battery

## Observation of In-Vehicle Lithium-Ion Secondary Batteries inspeXio SMX-225CT FPD HR Plus

The internal structure of a large rectangular battery developed for automotive applications was observed. When the inside was observed, the deformed negative electrode when the case was inserted can be seen. The structure of the connecting terminal can be observed as well.

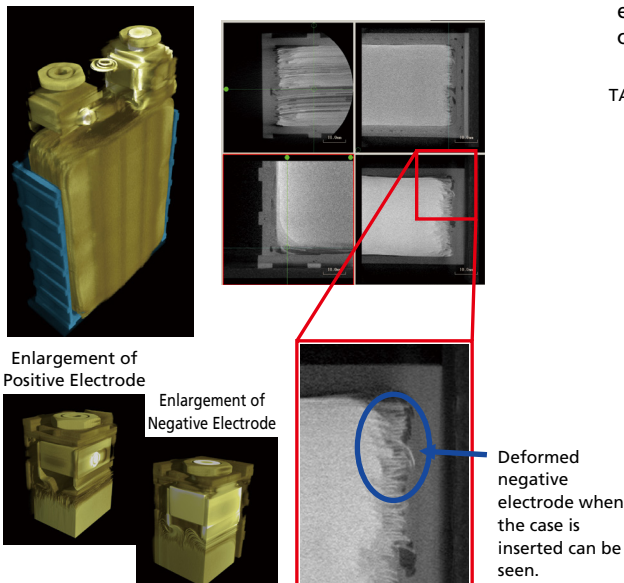


Fig. 3 In-Vehicle Lithium-Ion Battery

## Observation of Lithium Polymer Batteries inspeXio SMX-225CT FPD HR Plus

The following is an example of observing the inside of a lithium polymer battery sold as a mobile charger. The upper electronic device is an electronic circuit for detecting the state of charge and preventing ignition due to thermal runaway during overcharge. The TAB electrode section is bent so as not to be broken when cells are expanded and contracted.

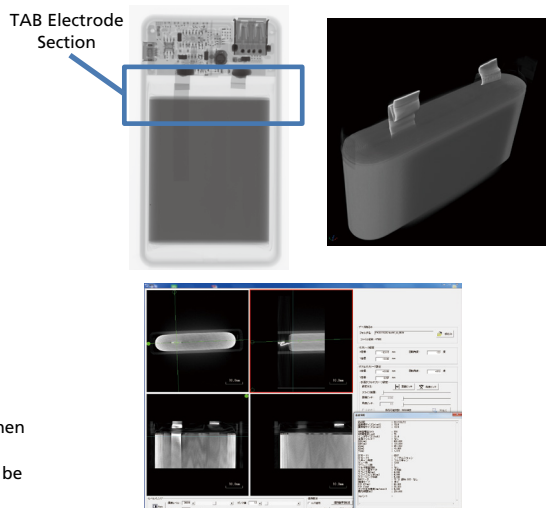


Fig. 4 Lithium Polymer Battery

# Analysis of Gases Generated Inside Batteries

## Analysis of Electrolytic Solution and Gases Generated from Cells GCMS-QP 2020 NX



Gas Chromatograph Mass Spectrometer  
GCMS-QP 2020 NX

An electrolytic solution for lithium-ion secondary batteries consists of organic solvents (mainly carbonates), electrolytes and additives. Analysis of the electrolytic solution and its degradation due to charging and discharging are important evaluation items in the development of lithium-ion secondary batteries. The GCMS-QP2020NX gas chromatograph mass spectrometer is useful for composition analysis of electrolytic solutions or analysis of denatured components of electrolytic solutions due to charging and discharging. This section introduces examples of the analysis of an electrolytic solution for a lithium-ion secondary battery using GCMS and gas generated from cells held at a high temperature.

### Analysis Results of Electrolytic Solution

The results obtained by measuring an electrolytic solution for a lithium-ion secondary battery are shown below. Dimethyl carbonate, ethylmethyl carbonate and ethylene carbonate were used as solvents and could be identified from library search results. Vinylene carbonate, used as an additive, was also identified (Fig. 1).

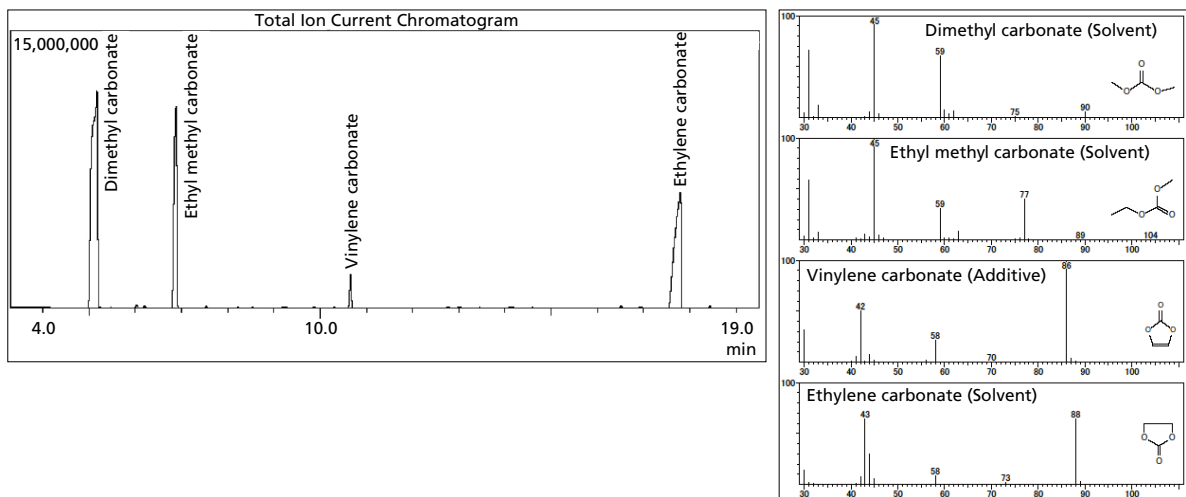


Fig. 1 Total Ion Current Chromatogram (TICC) of Electrolytic Solution and Mass Spectra of Each Component

### Analysis Results of Gas Generated from Cells

After an aluminum-laminated lithium-ion secondary battery was stored at 80 °C for 5 days, the generated gas was collected directly using a gas-tight syringe and analyzed qualitatively using GCMS. A large number of components derived from electrolytic solutions and components generated by modified solvents and additives could be identified. In addition, fluoride compounds derived from the electrolytic solutions could be identified from library searches (Fig. 2).

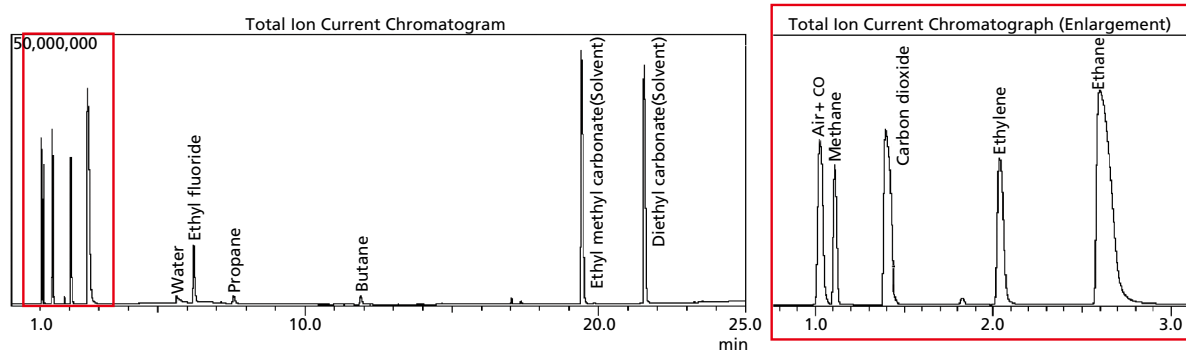


Fig. 2 Total Ion Current Chromatogram of Gas Generated from Cells (TICC)

# Analysis of Electrolytic Solution

## Analysis of Degradation Products in Electrolytes (Deteriorated Electrolytic Solution) HIC-ESP



Suppressor  
Ion Chromatograph  
for Anion Analysis  
HIC-ESP

Lithium hexafluorophosphate, which is used as an electrolytic solution for lithium-ion secondary batteries, is known to be hydrolyzed by a small amount of water contained in the electrolytic solution to form fluoride ions, etc. Since the fluoride ions produced by this hydrolysis affect battery performance, analysis of degradation products is important in the quality control process.

This section introduces an analysis of a new electrolytic solution and a deteriorated one taken from a battery which was used in an accelerated degradation test.

Figs. 1 and 2 show accelerated degradation test conditions and cycling characteristics. Figs. 3 and 4 are chromatograms of the new electrolytic solution and the deteriorated one taken from the battery used in the accelerated degradation test. Each sample was diluted 100 fold with purified water, filtered through a membrane filter and used for analysis. As a result of the analysis, fluoride ion (F) and difluorophosphate ion ( $\text{PO}_2\text{F}_2$ ) were detected in the deteriorated electrolytic solution.

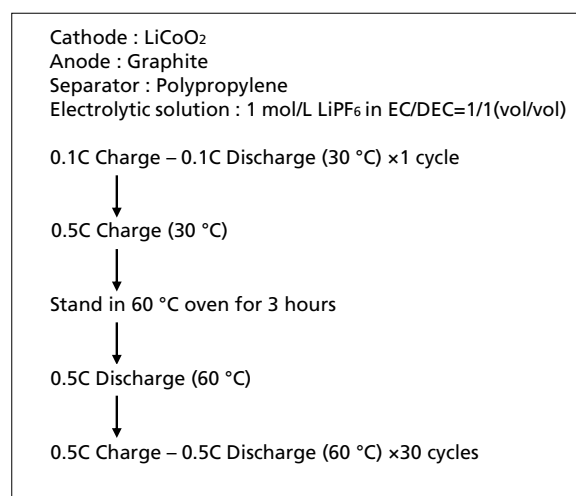


Fig. 1 Accelerated Degradation Test Conditions

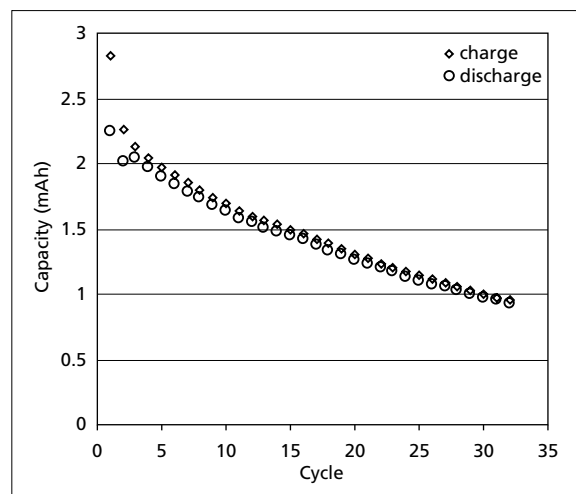


Fig. 2 Cycling Characteristics in Accelerated Degradation Tests

### Analysis Results of Electrolytic Solution

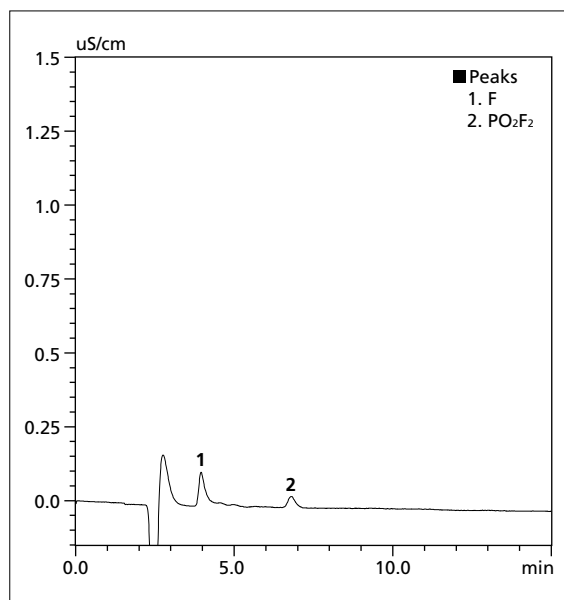


Fig. 3 Chromatogram of Electrolytic Solution (New)

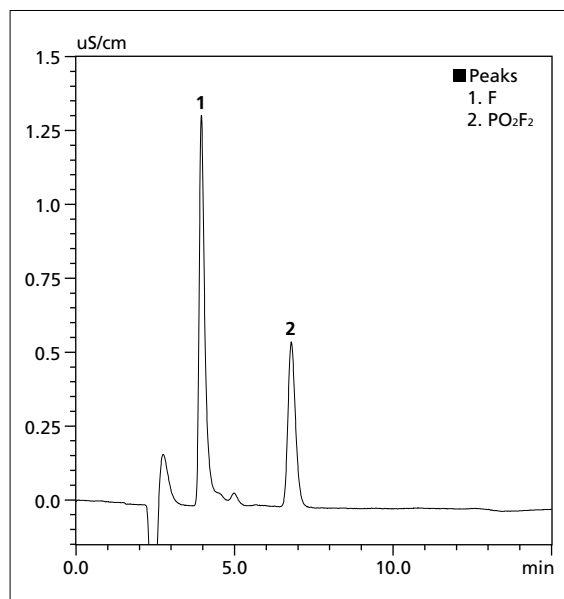


Fig. 4 Chromatogram of Electrolytic Solution (Deteriorated)

# Analysis of Negative Electrodes

## Shape Observation of Binder for Negative Electrodes in Electrolytic Solution/Force Curve Measurement SPM

This scanning probe microscope (SPM) scans the surface of a sample with a very small probe and observes the three-dimensional shape and local properties of the sample at high magnification. Unlike an electron microscope, the SPM can observe without a vacuum.

In this example, shapes of three kinds of polyacrylic acid binders in an electrolytic solution in which a battery actually worked, and in N<sub>2</sub> gas for reference, were observed using the SPM. Physical properties in the electrolytic solution were also measured (force curve measurement), and a suitable binder for Si negative electrode active materials was examined.

### Shape Observation in Electrolytic Solution

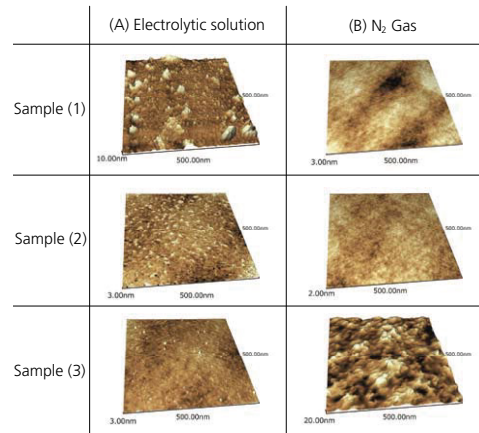
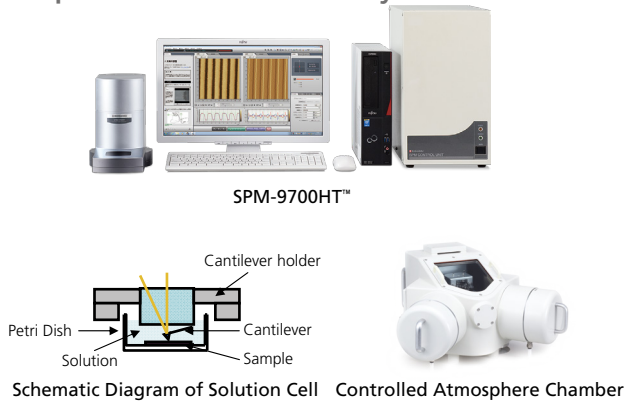


Fig. 1 Shapes in Electrolytic Solution and N<sub>2</sub> Gas (Magnification: 250,000 times)

As shown in Fig. 1, sample (1) had protrusions of about 10 nm in the electrolytic solution, while samples (2) and (3) had flat shapes. (Refer to (A)) This indicates that the binders of samples (2) and (3) were uniformly gelled in the electrolytic solution. On the other hand, in the N<sub>2</sub> gas, samples (1) and (2) had flat shapes and sample (3) had protrusions of 20nm. (Refer to (B)) The difference in results shows the importance of observing the samples in a real environment.

### Force Curve Measurement

A schematic diagram of force curve measurement is shown in Fig. 2. A force curve is obtained by measuring the force acting on the probe while changing the distance between the probe (cantilever) and the sample, and displaying it graphically. The amount of deformation and inclination when the probe is pushed into the sample makes it possible to compare and quantify the stiffness of the sample.

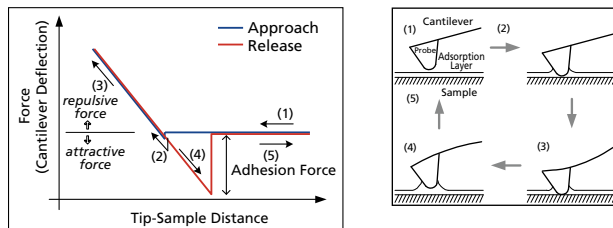


Fig. 2 Schematic Diagram of Force Curve Measurement

Figs. 3 to 5 show the measurement results of the force curve of samples (1), (2) and (3) in the electrolytic solution. The deflection of the cantilever when the probe was pushed into the samples about 15nm was measured between black inverted triangles (▼-▼). The deformation of the binder can be obtained from the difference between "indentation" and "deflection", indicating that sample (2) is the softest and sample (3) is the stiffest. (Refer to Table 1)

The results of the shape observation and the force curve measurement show the binder suitable for the Si negative electrode active materials is sample (3) due to its uniform shape, high rigidity, and little deformation in the electrolytic solution.

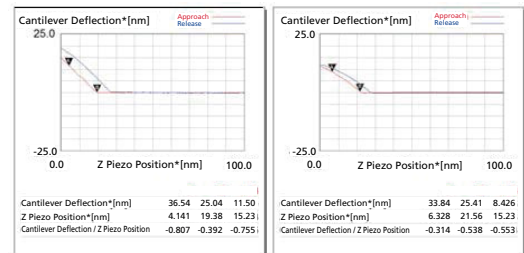


Fig. 3 Measurement Result of Sample (1)

Fig. 4 Measurement Result of Sample (2)

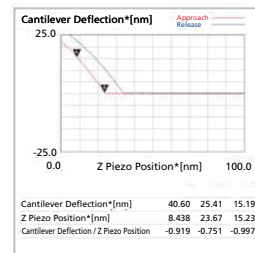


Fig. 5 Measurement Result of Sample (3)

Table 1. Measurement Results of Deformation

	(1)	(2)	(3)
Deformation (nm)	3.7	6.8	0

Deformation of Samples = Indentation - Deflection of Cantilever  
These samples were provided by Komaba Laboratory, Tokyo University of Science.

# Analysis of Separators

## Thermal Characterization of Separators

DSC-60Plus/TMA-60

### Melting Measurement of Separators using DSC



Differential Scanning Calorimeter DSC-60 Plus

Endothermic peaks, which were considered to be the melting of polyethylene, were measured at 100 to 150 °C in 3 different separators. There were differences in melting temperature and crystallinity (heat of fusion).

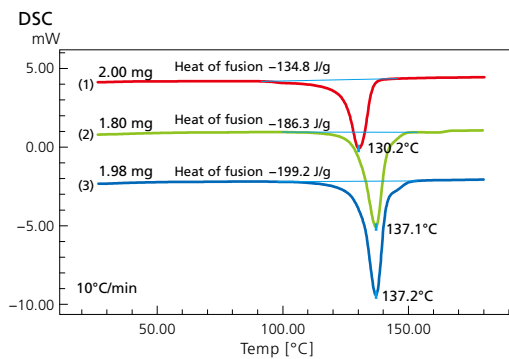


Fig. 1 DSC Measurement Results

### Shrinkage Measurement of Separators using TMA



Thermomechanical Analyzer TMA-60

Dimensional changes due to elongation or shrinkage were measured while a tensile load was applied in MD and TD directions of two separators. Comparison of samples (1) and (2) shows that sample (2) shrank at higher temperatures in both MD and TD and had better heat resistance. The shrinkage in TD was smaller than that in MD, and when the shrinkage between samples (1) and (2) in TD was compared, sample (1) was smaller than (2). It indicated that sample (1) was better for insulation when the battery's temperature increased.

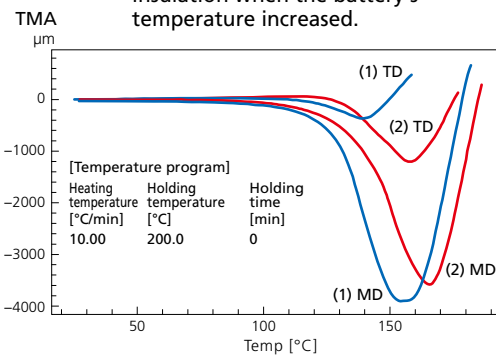


Fig. 2 TMA Measurement Results  
MD: Long-side Direction, TD: Short-side Direction

## Puncture Strength of Separators at Different Temperatures

AGX™-V

Separators not only ensure conductivity, which allows lithium ions to move smoothly between positive and negative electrodes, but also serve as an insulation to prevent direct contact between the positive and negative electrodes. Mechanical strength at high temperatures is a necessary property for safety, especially when a battery is charged. Here is an example of a puncture test to evaluate the mechanical strength at high temperatures.



Precision Universal Testing Machine AGX™-V Series



Images inside a Thermostatic Chamber

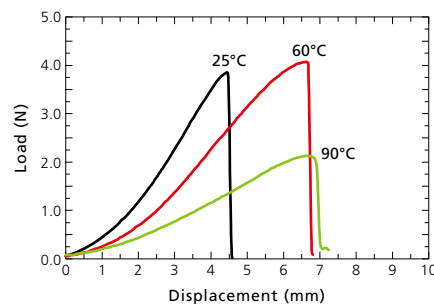


Fig. 1 Load-Displacement Curve

When the test results at 25°C and 60°C in Figure 1 and Table 1 were compared, the maximum load force was the same, but the maximum displacement at 60°C was larger than that at 25°C. When the test results at 60°C and 90°C were compared, the maximum displacement was the same, but the maximum load force at 90°C was greatly reduced. Based on the above, the separators used in this test had good heat resistance with a large elongation and no decrease in strength at a temperature of 60°C.

Table 1. Maximum Load Force and Maximum Displacement for Temperatures

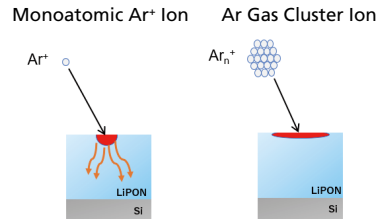
Temperature	Maximum Load Force (N)	Maximum Displacement (mm)
25 °C	3.85	4.45
60 °C	4.07	6.63
90 °C	2.13	6.68

## Depth Profiling of LiPON Films (Solid Electrolytes)

XPS

X-ray photoelectron spectroscopy (XPS) enables not only qualitative and quantitative analysis of elements present at approximately 10 nm on the surface of materials, but also analysis of chemical bonding states.

Using XPS, contamination removal and depth profiling of multilayer films can be performed by irradiating the sample surface with ions and performing sputter etching. Introduced here are examples of the analysis of the surface and depth profile of LiPON films formed by atomic layer deposition (ALD) using monoatomic Ar ions and Ar gas cluster ions.



In the case of Ar gas cluster ions, 500 to 3000 Ar atoms are converted into clusters and charged to a 1-valent positive charge, and the energy per 1 atom is as small as several 10 eV or less. On the other hand, monoatomic Ar ions irradiate samples at an energy of several keV per atom.

In the depth profiling with monoatomic Ar ions, the lithium concentration decreased as the ions proceeded and stabilized at about 25.5%. In addition, the lithium concentration increased significantly up to 44% in the vicinity of the LiPON/Si interface. In contrast, in the depth profiling with Ar gas cluster ions, it became stable at about 31%. These findings suggest that the results of LiPON depth profiling depend on the ion species irradiating the samples. (Refer to Figs. 1 and 2)

In the depth profiling of monoatomic Ar ions, the cause of low-concentration lithium is thought to be the lithium ions which were pushed into the LiPON due to a charge repulsion caused by irradiated Ar<sup>+</sup>, as shown in Fig. 3. The reason why this phenomenon did not appear in Ar gas cluster ions is likely because the number of positive charges was small for the Ar atoms irradiated. Furthermore, since the lithium ions pushed into the LiPON/Si interface could not move into the native Si oxide film, high-concentration lithium at the LiPON/Si interface is considered to be caused by the deposition at the LiPON/Si interface.

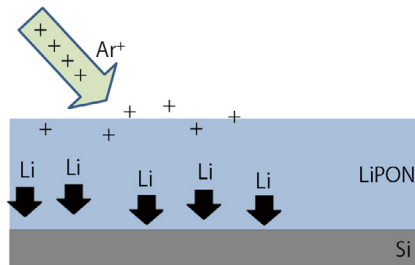


Fig. 3 Image of Lithium-Ion Transfer by Monoatomic Ar Ion Irradiation

From the above results, Ar gas cluster ions are considered to be suitable for the depth profiling of Li-containing battery materials such as LiPON because the depth profiling using Ar gas cluster ions can obtain more stoichiometrically accurate values than monoatomic Ar ions.

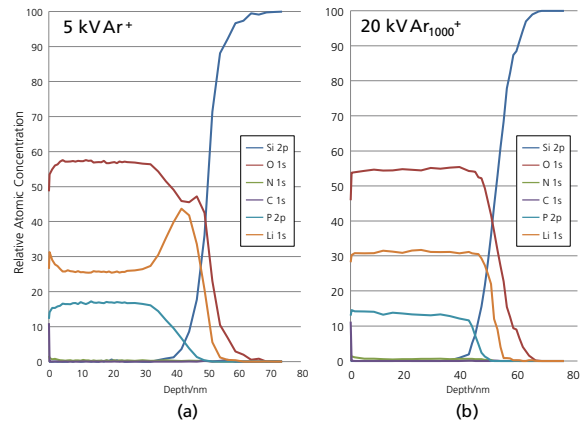


Fig. 1 Depth Profiling of 50nm-thick LiPON Thin Films using (a) Monoatomic Ar Ions (5kV Ar<sup>+</sup>) and (b) Ar Cluster Ions (20kV Ar 1000<sup>+</sup>)

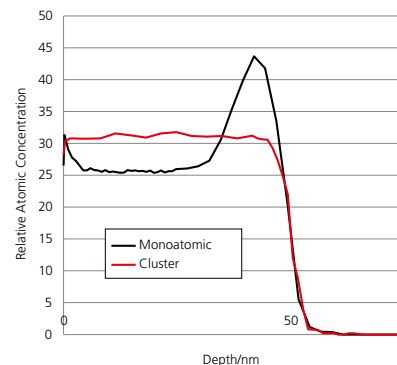


Fig. 2 Comparison of Monoatomic Profile (black) and Cluster Profile (red) of Lithium-Ion Concentration Extracted from (a) and (b) in Fig. 1

## Particle Size Distribution of Raw Material Powder (Solid Electrolytes) iSpect DIA-10

All-solid-state batteries are attracting attention as next-generation batteries that combine safety, high energy density, and long life. The key is said to be the development of solid electrolytes with high ionic conductivity, and it is necessary to understand the characteristics of raw material powder in order to develop the solid electrolytes. Here, an example of measuring the particle size and shape of fine raw material powder used for oxide-based solid electrolytes and measuring the particle size distribution is introduced.



Dynamic Particle Image Analysis System  
iSpect DIA-10

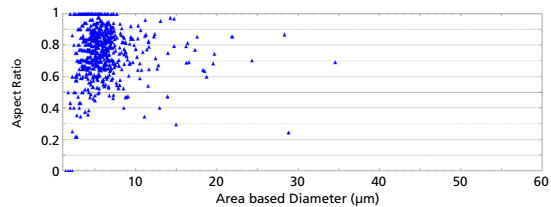
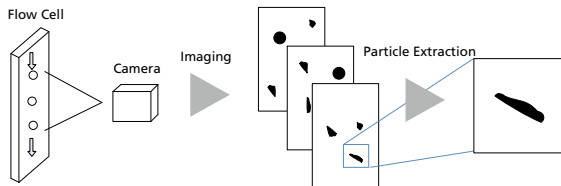


Fig. 1 Scattergram



Flowing particles are imaged and used to measure the size and shape of each particle by image analysis. Individual particle images can be saved.

The raw material powder for solid electrolytes contained many particles with a diameter of about 5 µm, and the shape was stable.

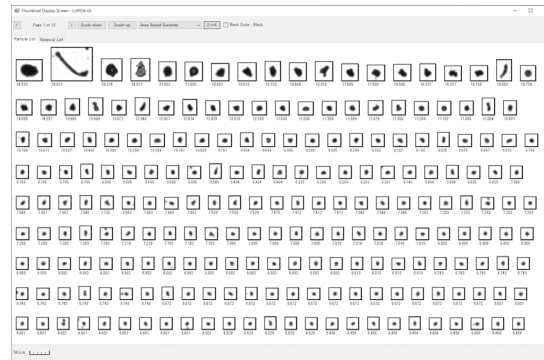


Fig. 2 Particle Image

## Compressive Strength of Raw Material Powder (Solid Electrolytes) MCT-510

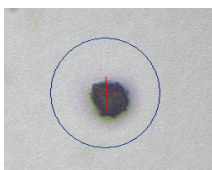
When solid electrolytes are manufactured, there may be a difference in formability due to a difference in the physical properties of particles. Compressing the powder used as a raw material for solid electrolytes and measuring the fracture strength from the fracture load make it possible to examine the correlation with easy formability.



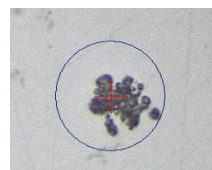
Micro Compression Tester  
MCT Series



Destruction can be checked in real time.



Before measurement



After destruction

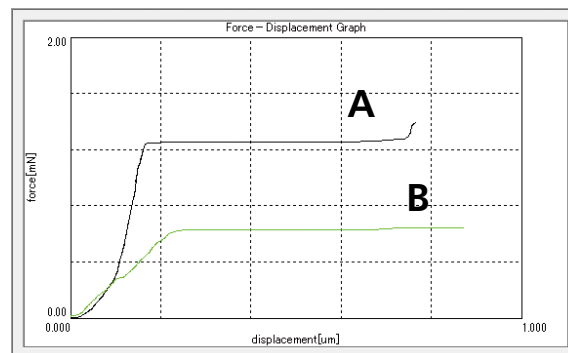


Fig. 1 Force-Displacement Graph

Table 1. Test Results

Sample Name	Fracture Load [mN]	Particle Size [µm]	Strength [MPa]
A	1.25	1.765	315
B	0.63	4.265	27

When particles A and B were compared, particle B had about 1/10 of the fracture strength and was relatively soft, indicating that particle B was easily formed into a solid electrolyte.

# Shimadzu's Analysis and Evaluation Technologies for Lithium-Ion Secondary Batteries

In addition to the applications described this brochure, Shimadzu provides analytical and evaluation solutions for lithium-ion secondary batteries.

Materials	Parts	Commonly Used Components	Evaluation Parameters (Analytical Devices)
Positive Electrode	Active Materials	LiCoO <sub>2</sub> (Lithium Cobalt Oxide) LiMn <sub>2</sub> O <sub>4</sub> (Lithium Manganate) LiNi <sub>x</sub> Mn <sub>y</sub> Co <sub>z</sub> O <sub>2</sub> Co (Ternary System)	Valence (Chemical Bond Analysis System) Composition (ICP, XRF) Crystallinity (XRD) Particle Size (Particle Size Distribution, Particle Image Analysis System) Electronic State (XPS) Specific Surface Area/Micropore Distribution (Gas Adsorption)
	Binder	Vinylidene Fluoride (PolyVinylidene DiFluoride; PVDF)	Molecular Weight Distribution (GPC) Surface Shape (SPM) Composition (FTIR)
	Conductive Aid	Carbon (Carbon Black, Acetylene Black, Graphite and others)	Crystallinity (XRD) Specific Surface Area/Micropore Distribution (Gas Adsorption)
Negative Electrode	Active Materials	Carbon, Graphite	Crystallinity (XRD) Particle Size (Particle Size Distribution, Particle Image Analysis System) Specific Surface Area/Micropore Distribution (Gas Adsorption) Compressive Strength (Micro Compression Tester)
	Trace amount of additives	Li, P, Cu, Na, Co, Ca, K etc.	Composition (ICP)
	Binder	SBR (Styrene-Butadiene Latex), CMC (Carboxymethyl Cellulose), Polyacrylic Acid, PVDF	Surface Shape (SPM) Structure (FTIR) Adhesive Strength (Testing Machine)
Separator		Polyolefin (High-Density Polyethylene)	Structure (FTIR) Surface Shape (SPM) Thermal Properties (DSC, TMA, TG) Tensile Strength (Testing Machine) Puncture Strength (Testing Machine)
Electrolytic Solution	Solvent	Ethylene Carbonate, Diethyl Carbonate, Ethyl Methyl Carbonate etc.	Composition (GC-MS, GC, LC)
	Electrolyte	LiPF <sub>6</sub> , LiBF <sub>4</sub>	Composition (Ion Chromatography System, LC, ICP)
	Additives	Vinylene Carbonate etc.	Composition (GC-MS, ICP)
Cell	Unit Module	-	Compressive Strength (Universal Testing Machine) Nail Penetration (Universal Testing Machine) Internal Observation (X-ray CT Scanner)

Xspecia and AGX are trademarks of Shimadzu Corporation.

These products have not been approved or certified as medical devices under the Pharmaceuticals and Medical Devices Act. They cannot be used for therapeutic diagnosis purposes or for the procedures. Please use genuine parts for repair parts and consumables to eliminate trouble. Please note that the appearance and specifications are subject to change for improvement without prior notice.



Shimadzu Corporation  
www.shimadzu.com/an/

#### For Research Use Only. Not for use in diagnostic procedures.

This publication may contain references to products that are not available in your country. Please contact us to check the availability of these products in your country. Company names, products/service names and logos used in this publication are trademarks and trade names of Shimadzu Corporation, its subsidiaries or its affiliates, whether or not they are used with trademark symbol "TM" or "®". Third-party trademarks and trade names may be used in this publication to refer to either the entities or their products/services, whether or not they are used with trademark symbol "TM" or "®". Shimadzu disclaims any proprietary interest in trademarks and trade names other than its own.

The contents of this publication are provided to you "as is" without warranty of any kind, and are subject to change without notice. Shimadzu does not assume any responsibility or liability for any damage, whether direct or indirect, relating to the use of this publication.